AIAA JOURNAL
Vol. 34, No. 8, August 1996

Behavior of Spinning Pretwisted Composite Plates Using a Nonlinear Finite Element Approach

Ravinder Bhumbla* and John B. Kosmatka†
University of California, San Diego, La Jolla, California 92093-0085

The behavior of spinning pretwisted plates is significantly different from that of spinning flat plates. The coupling between bending, twisting, and extension behavior, introduced because of the geometry of these plates, has a significant effect on their static and dynamic behavior. This, in conjunction with coupling due to material asymmetry, can result in fairly nonintuitive, though physically understandable, behavior. Since existing plate/shell finite elements have numerical deficiencies when modeling twisted plates, a six-node triangular element is developed for the analysis of spinning laminated composite structures. The element is based on a first-order shear deformable laminated plate theory. Complete cubic polynomials are used to represent the transverse deflections and complete quadratic polynomials are used to model the rotations and the in-plane displacements. Linear transformation relations are developed to move four nodes associated with transverse deflections to the element interior, and these nodes are then eliminated by using static and dynamic condensation to obtain a six-node element. The element is shown to be free of shear locking and superior to existing commercially available triangular elements. Numerical results are presented for the analysis of spinning laminated composite plates.

I. Introduction

INTEREST in the vibrational behavior of turbomachinery blades has led to a number of studies in the analysis of pretwisted blades. However, most of these studies have modeled the blades as cantilever pretwisted beams. This modeling is inaccurate for low-aspect-ratio blades that need to be modeled as pretwisted plates. Also, being essentially one-dimensional models, the beam models are unable to incorporate higher modes like those involving chordwise or edgewise bending. As these modes couple with bending modes for pretwisted blades, the beam model can lead to inaccurate results. A typical pretwisted plate is shown in Fig. 1.

It has been shown that pretwist causes an increase in torsional stiffness and decrease in bending stiffness. This was explained for beams by Zickel,[1] who pointed out that twist causes an inclination of lines parallel to the central line, reducing their radial distance from the initial twist axis. This causes smaller strain for a given curvature and also causes the stress in the direction of the lines to be concentrated more towards the beam axis. This reduces the resisting moment and, consequently, the bending stiffness. In the same way, resistance to torsion is increased with increasing pretwist.

MacBain[2] modeled spinning twisted isotropic cantilever plates using NASTRAN showing that pretwist resulted in a large increase in torsional frequencies, whereas it had little effect on bending frequencies and the bending frequencies were more strongly affected by the angular velocity than the torsional frequencies.

Sreenivasamurthy and Ramamurti[3,4] studied the vibration of rotating pretwisted low-aspect-ratio tapered cantilever plates. They observed an increase in frequency with rotational speeds for all vibration modes except edgewise bending. The decrease in edgewise bending frequency with speed is to be expected since the centrifugal stiffness term causes a decrease in the in-plane stiffness of the plate with increase in rotation speed.

Lapid et al.[5] presented results of experiments conducted at NASA Lewis for strains, deflection, and vibration behavior in nonspinning and spinning pretwisted laminated composite plates. For nonspinning pretwisted plates it was observed that pretwist had little effect on the first bending vibration frequency but resulted in a decrease in the frequency for higher bending modes. For torsional modes, it was noted that presence of pretwist greatly increased the vibration frequency. The location of the pretwist axis was shown to have little effect on the vibration frequencies. For spinning pretwisted plates, the study showed an increase with rotational speed for bending frequencies, whereas the torsional frequency showed a decrease with rotational speed. This behavior is observed in the current study.

Triangular plate elements are quite popular in plate/shell analyses because of their ability to model arbitrary plate and shell geometries. However, most existing elements have deficiencies that make them unacceptable for modeling thick plates or laminated composite plates that exhibit shear deformation behavior. Existing plate finite elements developed using the classical plate theory based on the Kirchhoff–Love hypothesis neglect the effect of shear deformation and cannot be used for thick or laminated composite plates. Elements based on first-order shear deformation theories overcome these shortcomings. However, many of these elements exhibit shear-locking behavior where techniques like reduced integration are used to overcome artificial stiffening.

Tessler and Hughes[6] developed a three-node triangular element using the Mindlin–Reissner theory. Full numerical integration was performed that eliminated the problem of rank deficiency. It was recognized that the shear-locking behavior was caused by the utilization of same order polynomials for rotations and displacements, which did not permit the shear strains to go to zero for thin plates. It was shown that the polynomials for the transverse displacement needed to be one order higher (quadratic) than those for rotations (linear). The transverse displacements at the midside nodes were condensed out by enforcing continuous shear strain constraints at every element edge. The resulting element needed finite element correction factors as well as shear correction factors.

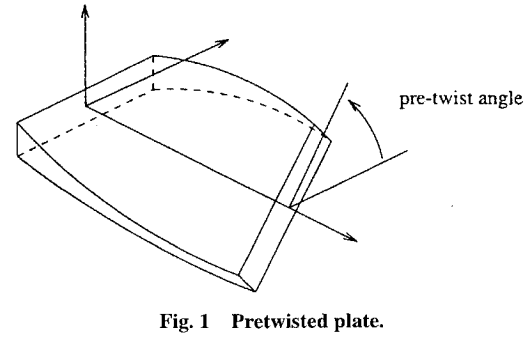

Fig. 1 Pretwisted plate.

Received Oct. 11, 1994; revision received April 5, 1995; accepted for publication Oct. 30, 1995. Copyright © 1995 by Ravinder Bhumbla and John B. Kosmatka. Published by the American Institute of Aeronautics and Astronautics, Inc., with permission.

*Graduate Research Assistant, Structural Systems Research, Department of Applied Mechanics and Engineering Sciences.

†Associate Professor, Structural Systems Research, Department of Applied Mechanics and Engineering Sciences.

Triangular plate elements based on complete cubic polynomials (10 nodes) for transverse deflections and complete quadratic polynomials (6 nodes) for rotations were developed by Yuan and Miller[7] and Kosmatka.[8] The former was developed for a flat orthotropic plate and modeled only out-of-plane bending behavior, whereas Kosmatka's element was based upon an isoparametric formulation and modeled both in-plane and out-of-plane behavior. These elements exhibit excellent behavior for thick and thin plates but are difficult to incorporate into existing commercially available finite element programs. Preliminary attempts[8] were made to transform this to a six-node element using geometry-based edge constraints that led to slight stiffening. Kosmatka[9] developed a fully conforming 6-node element from the above 13-node element by enforcing linear tangential strains along all edges.

The aim of the current paper is to develop nonlinear finite element techniques to study the static deflection and vibration behavior of spinning pretwisted plates. A 6-node triangle element is developed from the 13-node cubic element using linear transformations to move some of the edge nodes to the interior of the element and then use static and dynamic condensation (Guyan reduction) to eliminate degrees of freedom associated with these nodes. The resulting element, which is conforming in the rotations and the in-plan displacements but not in the transverse deflections, is shown to have the same accuracy as the original 13-node element. Results are presented to compare it with existing triangular elements and to show application of this element to the analysis of pretwisted plates.

II. Shear-Deformable Theory for Spinning Plates

For the first-order shear-deformation plate theory,[10,11] the displacements in the plane of the plate are assumed to be a linear function of the thickness coordinate z, and the transverse deflections are assumed to be constant through the thickness of the plate. The resulting displacements u, v, and w in the x, y, and z directions, respectively, can then be written as

$$\begin{aligned} u(x, y, z) &= u_0(x, y) + z\psi_x(x, y) \\ v(x, y, z) &= v_0(x, y) + z\psi_y(x, y) \\ w(x, y, z) &= w_0(x, y) \end{aligned} \tag{1}$$

where u_0, v_0, and w_0 are the displacements at the midplane of the plates; and, ψ_x and ψ_y are rotations about the y and $-x$ axes, respectively.

Making the von Kármán assumption that the products of derivatives of in-plane displacements are much smaller in magnitude than derivatives of displacements and products of derivatives of transverse displacement, one can write the strain displacement relations

$$\begin{Bmatrix} \epsilon_{xx} \\ \epsilon_{yy} \\ \gamma_{xy} \\ \gamma_{yz} \\ \gamma_{xz} \end{Bmatrix} = \begin{Bmatrix} \epsilon^0_{xx} \\ \epsilon^0_{yy} \\ \gamma^0_{xy} \\ \gamma^0_{yz} \\ \gamma^0_{xz} \end{Bmatrix} + z \begin{Bmatrix} \kappa^0_x \\ \kappa^0_y \\ \kappa^0_{xy} \\ 0 \\ 0 \end{Bmatrix} + \begin{Bmatrix} \epsilon^{NL}_{xx} \\ \epsilon^{NL}_{yy} \\ \gamma^{NL}_{xy} \\ 0 \\ 0 \end{Bmatrix} \tag{2}$$

where

$$\epsilon^0_{xx} = \frac{\partial u_0}{\partial x}, \qquad \epsilon^0_{yy} = \frac{\partial v_0}{\partial y}, \qquad \gamma^0_{xy} = \frac{\partial u_0}{\partial y} + \frac{\partial v_0}{\partial x} \tag{3a}$$

$$\gamma^0_{yz} = \psi_y + \frac{\partial w_0}{\partial y}, \qquad \gamma^0_{xz} = \psi_x + \frac{\partial w_0}{\partial x} \tag{3b}$$

$$\kappa^0_x = \frac{\partial \psi_x}{\partial x}, \qquad \kappa^0_y = \frac{\partial \psi_y}{\partial y}, \qquad \kappa^0_{xy} = \frac{\partial \psi_y}{\partial x} + \frac{\partial \psi_x}{\partial y} \tag{4}$$

$$\epsilon^{NL}_{xx} = \frac{1}{2}\left(\frac{\partial w_0}{\partial x}\right)^2, \quad \epsilon^{NL}_{yy} = \frac{1}{2}\left(\frac{\partial w_0}{\partial y}\right)^2, \quad \gamma^{NL}_{xy} = \frac{\partial w_0}{\partial x}\frac{\partial w_0}{\partial y} \tag{5}$$

where ϵ^0_{ij} and γ^0_{ij} are called the linear normal and shear strains, respectively; ϵ^{NL}_{ij} and γ^{NL}_{ij} are nonlinear normal and shear strains, respectively; and κ^0_{ij} are the plate curvatures.

For an orthotropic material having the material principal directions 1–2 at an angle θ to the corresponding plate coordinate axes x–y the constitutive relations are obtained to be

$$\begin{Bmatrix} \sigma_{xx} \\ \sigma_{yy} \\ \tau_{xy} \\ \tau_{yz} \\ \tau_{xz} \end{Bmatrix}^{(m)} = \begin{bmatrix} \bar{Q}_{11} & \bar{Q}_{12} & \bar{Q}_{16} & 0 & 0 \\ \bar{Q}_{12} & \bar{Q}_{22} & \bar{Q}_{26} & 0 & 0 \\ \bar{Q}_{16} & \bar{Q}_{26} & \bar{Q}_{66} & 0 & 0 \\ 0 & 0 & 0 & \bar{Q}_{44} & \bar{Q}_{45} \\ 0 & 0 & 0 & \bar{Q}_{45} & \bar{Q}_{55} \end{bmatrix}^{(m)} \begin{Bmatrix} \epsilon_{xx} \\ \epsilon_{yy} \\ \gamma_{xy} \\ \gamma_{yz} \\ \gamma_{xz} \end{Bmatrix} \tag{6}$$

where (m) denotes the mth ply in the laminated plate and $\bar{Q}^{(m)}_{ij}$ are the plane stress reduced stiffness coefficients for the laminate.

Assuming negligible transverse normal stress ($\sigma_{zz} = 0$), the strain energy U for an elastic system is given by

$$U = \frac{1}{2}\int_A \int_z \begin{Bmatrix} \sigma_{xx} \\ \sigma_{yy} \\ \tau_{xy} \end{Bmatrix}^T \begin{Bmatrix} \epsilon_{xx} \\ \epsilon_{yy} \\ \gamma_{xy} \end{Bmatrix} dx\, dA + \frac{1}{2}\int_A \int_z \begin{Bmatrix} \tau_{yz} \\ \tau_{xz} \end{Bmatrix}^T \begin{Bmatrix} \gamma_{yz} \\ \gamma_{xz} \end{Bmatrix} dz\, dA \tag{7}$$

where A is the plate area in the x–y plane.

Substituting Eq. (2) into the preceding equation results in

$$U = \frac{1}{2}\int_A \begin{Bmatrix} N_x \\ N_y \\ N_{xy} \\ M_x \\ M_y \\ M_{xy} \end{Bmatrix}^T \begin{Bmatrix} \epsilon^0_{xx} + \epsilon^{NL}_{xx} \\ \epsilon^0_{yy} + \epsilon^{NL}_{yy} \\ \gamma^0_{xy} + \gamma^{NL}_{xy} \\ \kappa^0_x \\ \kappa^0_y \\ \kappa^0_{xy} \end{Bmatrix} dA + \frac{1}{2}\int_A \begin{Bmatrix} Q_y \\ Q_x \end{Bmatrix}^T \begin{Bmatrix} \gamma^0_{yz} \\ \gamma^0_{xz} \end{Bmatrix} dA \tag{8}$$

where $\{N\}$ are the force resultants (normal force per unit edge length), $\{M\}$ are the moment resultants (moment per unit edge length), and $\{Q\}$ are the shear force resultants (shear force per unit edge length) acting on the plate, defined as follows:

$$\begin{Bmatrix} N_x \\ N_y \\ N_{xy} \end{Bmatrix} = \sum_{m=1}^{n} \int_{z_m}^{z_{m+1}} \begin{Bmatrix} \sigma_{xx} \\ \sigma_{yy} \\ \tau_{xy} \end{Bmatrix} dz,$$

$$\begin{Bmatrix} M_x \\ M_y \\ M_{xy} \end{Bmatrix} = \sum_{m=1}^{n} \int_{z_m}^{z_{m+1}} \begin{Bmatrix} \sigma_{xx} \\ \sigma_{yy} \\ \tau_{xy} \end{Bmatrix} z\, dz \tag{9}$$

$$\begin{Bmatrix} Q_y \\ Q_x \end{Bmatrix} = \sum_{m=1}^{n} \int_{z_m}^{z_{m+1}} \begin{Bmatrix} \tau_{yz} \\ \tau_{xz} \end{Bmatrix} dz$$

Using the constitutive relations (6) and the strain-displacement relations (2), the strain energy can alternatively be written as

$$U = \frac{1}{2}\int_A \begin{Bmatrix} \epsilon^0_{xx} + \epsilon^{NL}_{xx} \\ \epsilon^0_{yy} + \epsilon^{NL}_{yy} \\ \gamma^0_{xy} + \gamma^{NL}_{xy} \\ \kappa^0_x \\ \kappa^0_y \\ \kappa^0_{xy} \end{Bmatrix}^T [\bar{D}] \begin{Bmatrix} \epsilon^0_{xx} + \epsilon^{NL}_{xx} \\ \epsilon^0_{yy} + \epsilon^{NL}_{yy} \\ \gamma^0_{xy} + \gamma^{NL}_{xy} \\ \kappa^0_x \\ \kappa^0_y \\ \kappa^0_{xy} \end{Bmatrix} dA + \frac{1}{2}\int_A \begin{Bmatrix} \gamma^0_{yz} \\ \gamma^0_{xz} \end{Bmatrix}^T [\bar{A}] \begin{Bmatrix} \gamma^0_{yz} \\ \gamma^0_{xz} \end{Bmatrix} dA \tag{10}$$

where

$$[\bar{D}] = \begin{bmatrix} A_{11} & A_{12} & A_{16} & B_{11} & B_{12} & B_{16} \\ A_{12} & A_{22} & A_{26} & B_{12} & B_{22} & B_{26} \\ A_{16} & A_{26} & A_{66} & B_{16} & B_{26} & B_{66} \\ B_{11} & B_{12} & B_{16} & D_{11} & D_{12} & D_{16} \\ B_{12} & B_{22} & B_{26} & D_{12} & D_{22} & D_{26} \\ B_{16} & B_{26} & B_{66} & D_{16} & D_{26} & D_{66} \end{bmatrix}$$

with

$$(A_{ij}, B_{ij}, D_{ij}) = \sum_{m=1}^{n} \int_{z_m}^{z_{m+1}} \bar{Q}_{ij}(1, z, z^2)\, \mathrm{d}z \qquad i, j = 1, 2, 4, 5, 6$$

and

$$[\bar{A}] = \begin{bmatrix} k_{11}^2 A_{44} & k_{12}^2 A_{45} \\ k_{12}^2 A_{45} & k_{22}^2 A_{55} \end{bmatrix}$$

where k_{11}^2, k_{12}^2, and k_{22}^2 are the shear-correction factors needed to correctly scale the shear strain energy, and k_{12}^2 is zero for isotropic plates. For isotropic plates, the shear-correction factors k_{11}^2 and k_{22}^2 were obtained to be $\frac{5}{6}$ for static analysis by Reissner[10] and $\pi^2/12$ for vibrations by Mindlin.[11] The values for composite plates depend on the particular lay-up and are obtained on the basis of equilibrium equations involving transverse shear forces (see Whitney[12]).

The kinetic energy of the laminated composite plate is given by

$$T = \frac{1}{2} \int_A \int_h \rho \boldsymbol{V} \cdot \boldsymbol{V}\, \mathrm{d}z\, \mathrm{d}A \tag{11}$$

where ρ is the density of the plate that is assumed to be constant for any given lamina but may be different for different laminae and $\boldsymbol{V}$ is the velocity vector at any arbitrary point on the plate.

A reference coordinate system $(\hat{\imath}, \hat{\jmath}, \hat{k})$ is defined (Fig. 2). The reference coordinate system has one of its axes $(\hat{k})$ coincident with one of the axes of an inertial coordinate system (1, 2, 3) passing through the same origin and the other two axes coplanar with those of the inertial coordinate system. the reference coordinate system spins with an angular velocity Ω about the $\hat{k}$ axis. In addition, a plate coordinate system $\{\hat{e}_x, \hat{e}_y, \hat{e}_z\}$ is defined that is offset from the reference coordinate system by translations $\{h_i, h_j, h_k\}$ and rotations $(\beta_i, \beta_j, \beta_k)$ from the reference coordinate system. These angular offsets are also referred to as pitch (β_i) and precone (β_j) later in the study. Thus the plate is seen to be spinning with angular velocity Ω about the inertial coordinate system. Then the velocity $\boldsymbol{V}$ of an arbitrary point on the plate can be written in the inertial coordinate system as

$$\boldsymbol{V} = \frac{\partial \boldsymbol{r}}{\partial t} + \Omega \hat{k} \times \boldsymbol{r} \tag{12}$$

where $\boldsymbol{r} = (h_i\hat{\imath} + h_j\hat{\jmath} + h_k\hat{k}) + (x + u)\hat{e}_x + (y + v)\hat{e}_y + w\hat{e}_z$ is the offset of any point (x, y) on the plate from the spin axis, $\{h_i, h_j, h_k\}$ are the offsets (in the reference coordinate system) of the plate coordinate system from the spin axis, $\{\hat{\imath}, \hat{\jmath}, \hat{k}\}$ is the reference coordinate system, and $\{\hat{e}_x, \hat{e}_y, \hat{e}_z\}$ is the plate coordinate system.

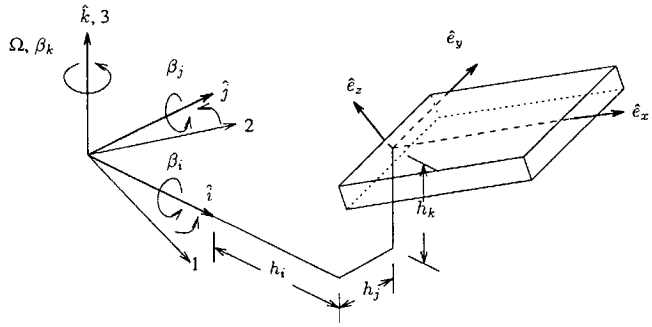

Fig. 2 Plate and reference coordinate systems.

The position vector $\boldsymbol{r}$ is obtained in the plate coordinate axes $\{\hat{e}_x, \hat{e}_y, \hat{e}_z\}$ using the transformation matrices $[T_{\beta_i}]$, $[T_{\beta_j}]$, and $[T_{\beta_k}]$, corresponding to the Euler angles β_i, β_j, and β_k, about the axes $\hat{\imath}$, $\hat{\jmath}$, and $\hat{k}$, respectively (Fig. 2),

$$\begin{Bmatrix} \hat{e}_x \\ \hat{e}_y \\ \hat{e}_z \end{Bmatrix} = [T_{\beta_k}][T_{\beta_j}][T_{\beta_i}] \begin{Bmatrix} \hat{\imath} \\ \hat{\jmath} \\ \hat{k} \end{Bmatrix} = [T_{LG}] \begin{Bmatrix} \hat{\imath} \\ \hat{\jmath} \\ \hat{k} \end{Bmatrix} \tag{13}$$

Using the preceding relations, the translational offsets of the plate coordinate system from the spin axis can be obtained in the plate coordinate system. Substituting the preceding relations into the expression for velocity of a point (12), and using the displacement field for the first-order theory (1), the velocity at any point on the plate can be written as

$$\begin{aligned} \boldsymbol{V} = {} & \hat{e}_x\{\dot{u}_0 + z\dot{\psi}_x + \Omega_y(h_z + w_0) - \Omega_z(h_y + y + v_0 + z\psi_y)\} \\ & + \hat{e}_y\{\dot{v}_0 + z\dot{\psi}_y(h_z + w_0) + \Omega_z(h_x + x + u_0 + z\psi_x)\} \\ & + \hat{e}_z\{\dot{w}_0 + \Omega_x(h_y + y + v_0 + z\psi_y) \\ & - \Omega_y(h_x + x + u_0 + z\psi_x)\} \end{aligned}$$

where

$$\{h_x, h_y, h_z\}^T = [T_{LG}]\{h_i, h_j, h_k\}^T$$

and

$$\{\Omega_x, \Omega_y, \Omega_z\}^T = [T_{LG}]\{0, 0, \Omega\}^T$$

The virtual work W_e done by external pressures acting on the plate is given by

$$\delta W_e = \int_A \begin{Bmatrix} p_x \\ p_y \\ p_z \end{Bmatrix}^T \begin{Bmatrix} \delta u_0 \\ \delta v_0 \\ \delta w_0 \end{Bmatrix} \mathrm{d}A \tag{14}$$

where p_x, p_y, and p_z are force per unit area acting in the x, y, and z directions, respectively.

The governing equations for the plate are obtained using Hamilton's principle:

$$0 = \int_{t_1}^{t_2} (\delta U - \delta T - \delta W_e)\, \mathrm{d}t \tag{15}$$

where U is the potential energy, T is the kinetic energy of the system, and δW_e is the virtual work of external forces.

Taking the variation of strain energy in Eq. (8),

$$\begin{aligned} \delta U = \int_A \Big[& N_x\left(\delta\epsilon_{xx}^0 + \delta\epsilon_{xx}^{NL}\right) + N_y\left(\delta\epsilon_{yy}^0 + \delta\epsilon_{yy}^{NL}\right) \\ & + N_{xy}\left(\delta\gamma_{xy}^0 + \delta\gamma_{xy}^{NL}\right) + M_x\delta\kappa_x^0 + M_y\delta\kappa_y^0 \\ & + M_{xy}\delta\kappa_{xy}^0 + Q_y\delta\gamma_{yz}^0 + Q_x\delta\gamma_{xz}^0\Big]\, \mathrm{d}A \end{aligned} \tag{16}$$

The strains and curvatures are integrated by parts to get displacement variations in the strain energy expression.

The variation of the kinetic energy is found to be

$$\begin{aligned} \int_{t_1}^{t_2} \delta T\, \mathrm{d}t = - \int_{t_1}^{t_2} \int_A \Big\{ & Z_{u_0}\delta u_0 + Z_{v_0}\delta v_0 + Z_{w_0}\delta w_0 \\ & + Z_{\psi_x}\delta\psi_x + Z_{\psi_y}\delta\psi_y \Big\}\, \mathrm{d}A\, \mathrm{d}t \end{aligned} \tag{17}$$

where Z_{u_0}, Z_{v_0}, Z_{w_0}, Z_{ψ_x}, and Z_{ψ_y} are inertial forces and moments described in Bhumbla and Kosmatka.[13]

Substituting the strain energy expression (16), the kinetic energy expression (17), and the external work expression (14) into Hamilton's principle and using the fact that the variations of the displacements u_0, v_0, w_0, ψ_x, and ψ_y vary independently of each other, one can obtain the following governing equations for the spinning plate:

$$\delta u_0: N_{x,x} + N_{xy,y} - Z_{u_0} = p_x$$

$$\delta v_0: N_{xy,x} + N_{y,y} - Z_{v_0} = p_y$$

$$\delta w_0: \frac{\partial}{\partial x}\left(N_x\frac{\partial w_0}{\partial x} + N_{xy}\frac{\partial w_0}{\partial y}\right) + \frac{\partial}{\partial y}\left(N_{xy}\frac{\partial w_0}{\partial x} + N_y\frac{\partial w_0}{\partial y}\right) + Q_{x,x} + Q_{y,y} - Z_{w_0} = p_z$$

$$\delta\psi_x: M_{x,x} + M_{xy,y} - Q_x - Z_{\psi_x} = 0$$

$$\delta\psi_y: M_{xy,x} + M_{y,y} - Q_y - Z_{\psi_y} = 0$$

III. Triangular Element Development

A new triangular plate/shell finite element was developed for this study based on the 13-node plate developed by Yuan and Miller[7] and Kosmatka.[8] The development for the 13-node (virgin) element is given next followed by development of a 6-node element based on the virgin element.

The triangular element was developed using quadratic interpolation functions for the in-plane displacements u_0 and v_0 and for the rotations ψ_x and ψ_y. Cubic interpolation functions were used for the transverse deflections w_0. This formulation is required to ensure that the energy corresponding to shear deformation goes to zero as the plate becomes thin.

A complete quadratic polynomial has six coefficients and thus requires six nodal values. Similarly a complete cubic polynomial needs 10 constants (and consequently 10 nodal values) to define it. These polynomials have been developed using area coordinates.[14] The use of area coordinates has some advantages that include automatic specification of element nodes, generation of complete polynomials for each order polynomial, and simple explicit expressions for shape functions that facilitate integration in this coordinate system.

Thus,

$$u_0 = \{\phi\}\{U\}, \quad v_0 = \{\phi\}\{V\}, \quad w_0 = \{\chi'\}\{W'\}$$
$$\psi_x = \{\phi\}\{\Psi_x\}, \quad \psi_y = \{\phi\}\{\Psi_y\} \tag{18}$$

where $\{\phi\}$ are the 6 quadratic interpolation functions and $\{\chi'\}$ are the 10 cubic interpolation functions; $\boldsymbol{U}$, $\boldsymbol{V}$, Ψ_x, and Ψ_y are the nodal values of the in-plane displacements u_0 and v_0 and the rotations ψ_x and ψ_y, respectively; and $\boldsymbol{W}'$ are the nodal values of the transverse deflections w_0.

Using the strain-displacements relations for the first-order theory (2) and the preceding interpolations, the following relationship is obtained between the midplane strains and curvatures and the displacements:

$$\begin{Bmatrix} \epsilon^0_{xx} + \epsilon^{NL}_{xx} \\ \epsilon^0_{yy} + \epsilon^{NL}_{yy} \\ \gamma^0_{xy} + \gamma^{NL}_{xy} \\ \kappa^0_x \\ \kappa^0_y \\ \kappa^0_{xy} \end{Bmatrix} = \left[B_0 + \frac{1}{2}B_{NL}\right] \begin{Bmatrix} \boldsymbol{U} \\ \boldsymbol{V} \\ \boldsymbol{W}' \\ \Psi_x \\ \Psi_y \end{Bmatrix} \tag{19}$$

where $[B_0]$ and $[B_{NL}]$ are matrices of derivatives of shape functions corresponding to linear and nonlinear strains, respectively, defined as follows:

$$[B_0] = \begin{bmatrix} \phi_{,x} & 0 & 0 & 0 & 0 \\ 0 & \phi_{,y} & 0 & 0 & 0 \\ \phi_{,y} & \phi_{,x} & 0 & 0 & 0 \\ 0 & 0 & 0 & \phi_{,x} & 0 \\ 0 & 0 & 0 & 0 & \phi_{,y} \\ 0 & 0 & 0 & \phi_{,y} & \phi_{,x} \end{bmatrix}$$

$$[B_{NL}] = \begin{bmatrix} 0 & 0 & \frac{\partial w}{\partial x}\chi'_{,x} & 0 & 0 \\ 0 & 0 & \frac{\partial w}{\partial y}\chi'_{,y} & 0 & 0 \\ 0 & 0 & \frac{\partial w}{\partial y}\chi'_{,x} + \frac{\partial w}{\partial y}\chi'_{,y} & 0 & 0 \\ 0 & 0 & 0 & 0 & 0 \\ 0 & 0 & 0 & 0 & 0 \\ 0 & 0 & 0 & 0 & 0 \end{bmatrix}$$

The terms involving derivatives of the transverse deflection w required for the preceding matrices are the terms generating nonlinear strains. The derivatives of w_0 are evaluated using the values of w_0 obtained from the previous iteration in the nonlinear analysis.

Similarly,

$$\begin{Bmatrix} \gamma_{yz} \\ \gamma_{xz} \end{Bmatrix} = [B_s] \begin{Bmatrix} \boldsymbol{U} \\ \boldsymbol{V} \\ \boldsymbol{W}' \\ \Psi_x \\ \Psi_y \end{Bmatrix} \tag{20}$$

where $[B_s]$ is a matrix of shape functions corresponding to the transverse shear strains defined as

$$[B_s] = \begin{bmatrix} 0 & 0 & \chi'_{,y} & 0 & \phi \\ 0 & 0 & \chi'_{,x} & \phi & 0 \end{bmatrix}$$

The resulting 13-node, 34-degree-of-freedom element[7,8] (Fig. 3), henceforth referred to as the virgin element, was developed based on this formulation and using the first-order shear deformation plate theory. The shape functions for this element are the usual quadratic and cubic shape functions in area coordinates. The virgin element is fully integrated and displayed excellent characteristics, including absence of shear locking, which is a common failing of many elements based on shear-deformation plate theories.

A. Ten-Node Element

The virgin element displays excellent behavior for thick and thin plates, but the nodes for transverse deflections do not coincide with those for the in-plane displacements and rotations. Thus the midside nodes (4, 5, and 6) of the triangle do not model transverse deflections, whereas the nodes 7–13 do not model the in-plane displacements and rotations. This increases the number of nodes in the element, which makes the element computationally expensive and difficult to program.

Simple transformations were developed to move three of the transverse deflection nodes to the element midsides and three to the element interior. The locations of the interior nodes were selected to obtain proper element behavior. It was observed that if the nodal configuration results in any four element nodes being collinear, the resulting transformation is singular making it unacceptable. So the symmetrical configuration with nodes 7, 8, and 9 having area coordinates as permutations of $(\frac{1}{6}, \frac{1}{6}, \frac{2}{3})$ had to be abandoned. A triangular element with interior nodes 7 $(\frac{1}{3}, \frac{1}{2}, \frac{1}{6})$, 8 $(\frac{1}{6}, \frac{1}{3}, \frac{1}{2})$, and 9 $(\frac{1}{2}, \frac{1}{6}, \frac{1}{3})$, (Fig. 3) was selected.

Since the nodes used for modeling the in-plane displacements and rotations for this element are the same as those used for the virgin elements, the corresponding shape functions for these displacement variables for this element are identical to those for the virgin element.

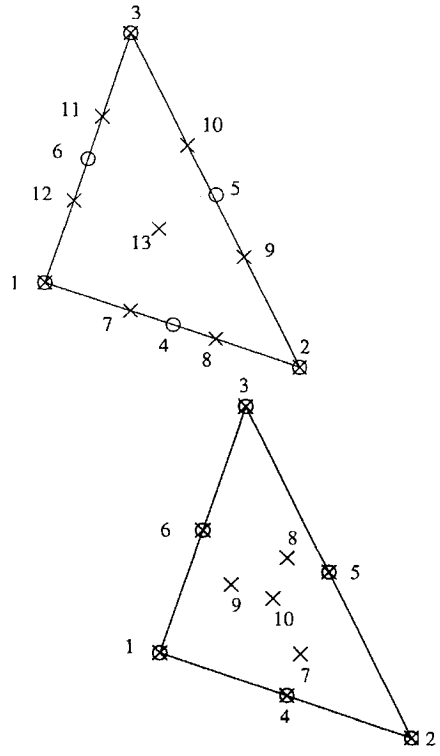

Fig. 3 Virgin (13-node) and 10-node triangular elements: ○, nodes for u, v, ψ_x, ψ_y and ×, nodes for w.

For the transverse deflection, the shape functions corresponding to the new nodal locations are obtained using the cubic shape functions for transverse deflections for the virgin element as described later. For the virgin element, the transverse deflection w_0 at any point in the element can be written as a linear combination of the nodal deflections,

$$w_0(L_1, L_2, L_3) = \{\chi'\}^T\{W'\} \tag{21}$$

where $\{W'\} = \{w_1, w_2, w_3, w_7, w_8, w_9, w_{10}, w_{11}, w_{12}, w_{13}\}^T$ are the nodal deflections and $\{\chi'\} = \{\chi'_1, \chi'_2, \chi'_3, \chi'_7, \chi'_8, \chi'_9, \chi'_{10}, \chi'_{11}, \chi'_{12}, \chi'_{13}\}^T$ are the cubic shape functions for the virgin element.

In particular, the deflections at the new nodal positions can be written as a linear combination of the nodal deflections of the virgin element. Thus,

$$\{W'\} = [\bar{T}_w]\{W\} \tag{22}$$

where

$$\{W\}^T = \{w_1, w_2, w_3, w_4, w_5, w_6, w_7, w_8, w_9, w_{10}\}$$

and

Substituting for $\{W'\}$ from Eq. (22) into Eq. (21),

$$w_0(L_1, L_2, L_3) = \{\chi'\}^T[\bar{T}_w]\{W\}$$

or

$$w_0(L_1, L_2, L_3) = \{\chi\}^T\{W\} \tag{23}$$

where

$$\{\chi\} = \{\chi'\}^T[\bar{T}_w]$$

Thus, $\{\chi\}$ are the equivalent shape functions based on the new nodal configuration. This new element has the same number of degrees of freedom, 34, as the virgin element. However, it has 10 nodes as opposed to the 13 nodes for the virgin element.

The in-plane displacements and the rotations for the element are modeled by quadratic polynomials. Along any edge of the element the shape functions are quadratic functions of distance along that edge. Since each edge of the plate has three nodes, the exact number required to define a quadratic polynomial, the in-plane displacement, and the rotations at any point along the edge are uniquely defined in terms of the corresponding values at the nodes along the edge. Thus for any other element sharing the edge, the in-plane displacements and rotations will be identical. This ensures that the element is conforming with respect to the in-plane displacements, u_0 and v_0 and rotations, ψ_x and ψ_y.

However, the transverse deflections are interpolated by cubic functions that have four independent coefficients. So at least four nodes are required to define such a function. In the current 10-node element each edge has only three nodes along any edge and there are four nodes in the interior. So transverse deflection at a point along any edge cannot be determined solely by the nodal values along the edge but instead depends on values at other nodes in the element away from the edge under consideration. Because of this, two elements sharing an edge need not have the same transverse deflections along the edge. Thus the element developed is nonconforming in the transverse deflection, w_0. It has been shown in the current study that negligible errors are introduced by this technique.

B. Six-Node (Condensed) Element

The 10-node element obtained earlier was condensed statically to eliminate the transverse deflections, w_0, modeled by the four nodes in the interior of the element. The resulting element has only six nodes, carrying exactly five degrees of freedom each, namely, u_0, v_0, w_0, ψ_x, and ψ_y. Though this 30 degree-of-freedom triangular element requires exactly the same number of computations for evaluating the element matrices as the original 10-node triangle, it has the advantage of having fewer global degrees of freedom.

The static condensation is carried out in the usual fashion as follows. Let

$$[K_e]\{q\} = \{F_e\}$$

be the usual equation for static analysis of the element. Then the stiffness matrix, the forces, and the degrees of freedom are partitioned

$$[\bar{T}_w] = \begin{bmatrix}
1 & 0 & 0 & 0 & 0 & 0 & 0 & 0 & 0 & 0 \\
0 & 1 & 0 & 0 & 0 & 0 & 0 & 0 & 0 & 0 \\
0 & 0 & 1 & 0 & 0 & 0 & 0 & 0 & 0 & 0 \\
4/21 & 1/21 & 2/21 & 12/7 & 16/21 & 4/21 & -24/7 & -20/7 & -12/7 & 6 \\
-5/63 & 4/63 & -2/21 & 4/63 & -16/21 & -4/21 & 24/7 & 20/7 & 12/7 & -6 \\
2/21 & 4/21 & 1/21 & 4/21 & 12/7 & 16/21 & -12/7 & -24/7 & -20/7 & 6 \\
-2/21 & -5/63 & 4/63 & -4/21 & 4/63 & -16/21 & 12/7 & 24/7 & 20/7 & -6 \\
1/21 & 2/21 & 4/21 & 16/21 & 4/21 & 12/7 & -20/7 & -12/7 & -24/7 & 6 \\
4/63 & -2/21 & -5/63 & -16/21 & -4/21 & 4/63 & 20/7 & 12/7 & 24/7 & -6 \\
0 & 0 & 0 & 0 & 0 & 0 & 0 & 0 & 0 & 1
\end{bmatrix}$$

in terms of degrees of freedom to be eliminated and those to be retained.

Thus,

$$\begin{bmatrix} [K_e^{bb}] & [K_e^{bc}] \\ [K_e^{cb}] & [K_e^{cc}] \end{bmatrix} \begin{Bmatrix} q^b \\ q^c \end{Bmatrix} = \begin{Bmatrix} F_e^b \\ F_e^c \end{Bmatrix}$$

where

$$\{q^c\} = \{w_7, w_8, w_9, w_{10}\}^T$$

are the degrees of freedom that need to be condensed out (eliminated).

By simple matrix manipulation, it can be seen that

$$[K_e^{bb}]^*\{q^b\} = \{F_e^b\}^* \tag{24}$$

where

$$[K_e^{bb}]^* = [K_e^{bb}] - [K_e^{cb}]^T[K_e^{cc}]^{-1}[K_e^{cb}] = [T]^T[K_e][T]$$

$$\{F_e^b\}^* = \{F_e^b\} - [K_e^{cb}]^T[K_e^{cc}]^{-1}\{F_e^c\} = [T]^T\{F_e\}$$

are the condensed element stiffness matrix and condensed element force, respectively, and

$$[T] \equiv \begin{bmatrix} [I] \\ -[K_e^{cc}]^{-1}[K_e^{cb}] \end{bmatrix}$$

is the transformation matrix for static condensation, $[I]$ being the identity matrix.

This condensation is an exact process and does not introduce any approximation (i.e., stiffening) for static analysis. The nodal degrees of freedom $\{q^b\}$ are determined by solving the global equations of motion. The four unknown interior degrees of freedom $\{q^c\}$ can then be obtained by using the relation

$$\{q^c\} = [K_e^{cc}]^{-1}[\{F_e^c\} - [K_e^{cb}]\{q^b\}] \tag{25}$$

The transformations used for static condensation are now used to reduce the element mass and damping matrices.[15]

The resulting elemental equations of motion are

$$[M_e^{bb}]^*\{\ddot{q}^b\} + [C_e^{bb}]^*\{\dot{q}^b\} + [K_e^{bb}]^*\{q^b\} = 0$$

where

$$[M_e]^* = [T]^T[M_e][T], \qquad [C_e]^* = [T]^T[C_e][T]$$

and $[T]$ is the transformation defined previously. The stiffness matrix obtained from this dynamic condensation is identical to that obtained from the static condensation. The term $[M_e^{bb}]^*$ is the condensed element mass matrix and $[C_e^{bb}]^*$ is the condensed element damping matrix.

The preceding analysis is generalized for pretwisted analysis by incorporating a small spurious stiffness[16] corresponding to the in-plane rotation θ_z. The spurious stiffness is chosen to be 10^{-4} times the smallest term on the diagonal of the element stiffness matrix. This has the effect that the corresponding element stiffness is nonsingular while ensuring that the spurious stiffness corresponding to θ_z does not have any significant effect on the element stiffness. The resulting mass and stiffness matrices are then transformed from the elemental coordinates via orthonormal transformation and incorporated into global matrices.

IV. Solution Procedure

The equations relating normal and shear strains to nodal displacements (18–20) are substituted into the Hamilton's principle (15) to obtain the elemental equations of motion that are then assembled to obtain the global equations of motion for the structure:

$$[M]\{\ddot{q}\} + [C]\{\dot{q}\} + \left([K^L] + \tfrac{1}{2}[K^{NL}]\right.$$

$$\left. + [K^G] + [K^S] + [K^{CF}]\right)\{q\} - \{F^{CF}\} = 0 \tag{26}$$

where $[K^L]$, $[K^{NL}]$, $[K^G]$, and $[K^S]$ are the usual linear stiffness, nonlinear stiffness, geometric stiffness, and shear stiffness matrices, respectively; $[M]$, $[C]$, and $[K^{CF}]$ are the global mass, Coriolis, and centrifugal stiffness matrices, respectively; and $\{F^{CF}\}$ is the global force vector. All of the matrices are symmetric except $[C]$, which is skew symmetric and $[K^{NL}]$, which is unsymmetric and depends upon the magnitude of the displacement variable q. These matrices are described in the Appendix.

The solution of the preceding equation is obtained by assuming the motion of the plate to be composed of two components: a static (time-independent) converged deflection $\{q_s\}$ due to the centrifugal forces and a harmonic motion $\{\delta(t)\}$ about this converged position. The equations of motion (26) are solved in two steps. First, the nonlinear static deformed position $\{q_s\}$ due to centrifugal forces is obtained, and then the dynamic motion $\{\delta(t)\}$ about this static converged solution is solved.

Neglecting the time-dependent motion in (26), the following static geometrically nonlinear equations of motion are obtained:

$$\left([K^L] + \tfrac{1}{2}[K^{NL}(q_s)] + [K^G] + [K^S] + [K^{CF}]\right)\{q_s\} = \{F^{CF}\} \tag{27}$$

These nonlinear equations of motion are solved using the Newton–Raphson technique. Once the static converged solution $\{q_s\}$ is obtained, Eq. (27) is substituted into Eq. (26). Taking the Taylor series expansion of $[K^{NL}(q_s)]$ about $\{q_s\}$, and neglecting the products of the perturbation quantities (i.e., $\delta \cdot \delta \approx 0$), the following equations of motion are obtained:

$$[M]\{\ddot{\delta}\} + [C]\{\dot{\delta}\} + [K^T]\{\delta\} = 0 \tag{28}$$

where $[K^T]$ is the usual tangent stiffness matrix.[17]

This is the standard form of equations of motion for undamped free vibrations of spinning structures. This is rewritten in the following form for the usual eigenvalue analysis:

$$[A]\{y\} - [B]\{\dot{y}\} = 0 \tag{29}$$

where

$$[A] = \begin{bmatrix} [M] & [0] \\ [0] & [K]^T \end{bmatrix}, \qquad [B] = \begin{bmatrix} [0] & [M] \\ -[M] & -[C] \end{bmatrix}$$

$$\{y\} = \begin{Bmatrix} \{\dot{\delta}\} \\ \{\delta\} \end{Bmatrix}$$

Assuming the solution to be harmonic, $\delta(t) = e^{\lambda t}$

$$[B]^{-1}[A]\{y\} = \lambda[I]\{y\}$$

and so the eigenvalues of $[B]^{-1}[A]$ are the eigenvalues of the system.

V. Numerical Results

Numerical results are presented to compare the behavior of the element developed with existing elements and to show the application of this element to the analysis of spinning pretwisted plates. The isotropic material used in some of the results is aluminum with the following material properties: $E = 69$ Gpa, $\nu = 0.3$, and $\rho = 2713$ kg/m^3. The composite material studied was graphite/epoxy with the following orthotropic material properties: $E_1 = 154.9$ GPa, $E_2 = E_3 = 10.01$ GPa, $G_{12} = G_{13} = 6.33$ GPa, $G_{23} = 3.58$ GPa, $\nu_{12} = \nu_{13} = 0.25$, $\nu_{23} = 0.40$, and $\rho = 1660.0$ kg/m^3.

Both the 10-node and 6-node (virgin) triangular elements successfully passed the standard patch tests of Refs. 7 and 9 and had the requisite 6 rigid-body modes (eigenvalue and eigenvector analysis of the element stiffness matrix) over an extreme range of aspect ratios.

A. Triangular Element Behavior

A comparison is made between results obtained by the present finite element model and those obtained by MSC/NASTRAN using the CTRIA6 element for a uniformly loaded square [0/90/0] graphite/epoxy laminated composite plate simply supported on all four sides. The plate has the dimensions $a = b = 0.1$ m. For the laminated composite plate, the shear correction factors were $k_{11} = 0.7925$, $k_{12} = 0$, and $k_{22} = 0.6966$. These values for the shear correction factors were obtained internally in the MSC/NASTRAN code and were used here to be consistent.

Effects of mesh refinement behavior, linear/nonlinear behavior, and the plate thickness on the static deflection behavior of these plates are presented. Because of the symmetric nature of the problem, only a quarter plate needs to be modeled to capture the behavior of the full plate. The mesh configurations for the quarter plate are shown in Fig. 4. The transverse deflection at the center of the simply supported plate is nondimensionalized with respect to the first-order shear deformation plate theory (FSDPT) based series solution. The current element is seen to converge faster than the MSC/NASTRAN CTRIA6 element for this thin ($a/h = 20$) laminated plate.

The effect of thickness on the linear static behavior of a simply supported square plate is presented in Fig. 5. The results have been nondimensionalized with respect to the FSDPT series solution for this problem. The thickness to length ratio a/h was allowed to vary from 1 to 1000 to see the behavior of very thick to very thin plates. As can be seen in Fig. 5, for both thin and thick plates the finite element solution converges to that obtained from the series solution. The triangular elements developed do not exhibit any shear locking behavior for very thin plates. The solution from the virgin and the 6-node triangular element is seen to match the series solution to 4 significant places for aspect ratios of up to 1000. However, at aspect ratio 200, the NASTRAN solution is seen to be about 4% stiffer than the series solution. Moreover, the NASTRAN solution becomes unstable for aspect ratios greater than 200.

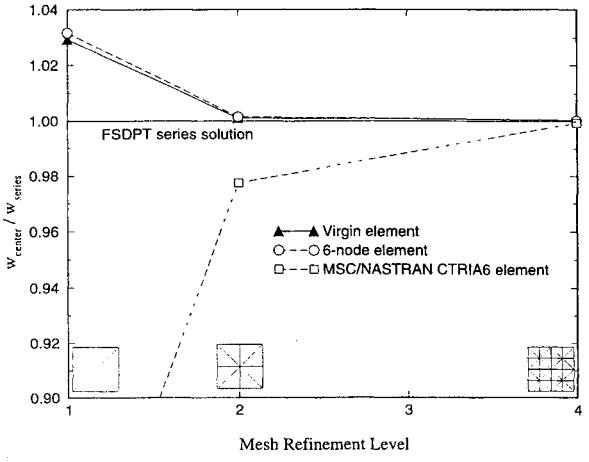

Fig. 4 Convergence behavior for thin square simply supported [0/90/0] composite plate, $a/h = 20$.

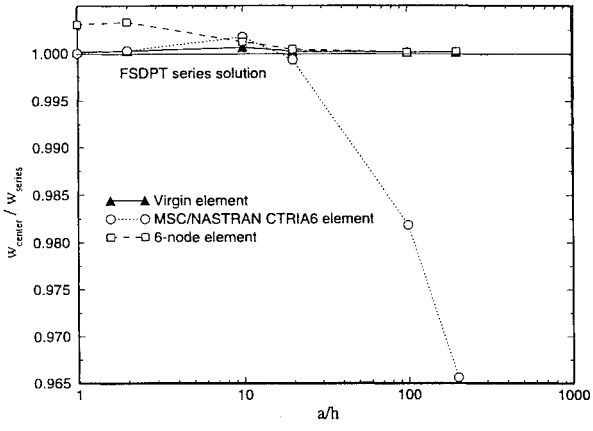

Fig. 5 Thickness effects for square laminated composite plate, uniformly distributed load = 1 N/m^2.

B. Nonspinning Pretwisted Plates

The effect of pretwist angle on the vibration behavior of a square isotropic cantilever plate is compared with Ref. 18 in Fig. 6 for the lower vibration modes (first bending, first torsion, and second bending). The vibration frequencies have been nondimensionalized by the relation $\bar{\omega} = \omega a^2\sqrt{(\rho h/D)}$. The error bars in the graph represent the range of results presented in the NASA study based on finite element analyses using beam elements, flat shell, and curved shell elements and solid elements along with experimental results. As can be seen from the graph and the tabulated comparison, there is excellent agreement between the current study and Ref. 18. For the lower modes, error bars are not visible for some pretwist angles because of their small range and their close agreement with the current results. These error bars are hidden behind the corresponding symbols. The graph also shows the effect of initial pretwist on the tip twist of the same pretwisted plate subjected to a uniform axial load of 10 kN/m. It is seen that the tip twist attains a maximum magnitude for an initial pretwist of 15–30 deg and then decreases in magnitude.

C. Spinning Plates

The importance of inclusion of geometric nonlinearities for the vibration analysis of spinning plates is shown in Fig. 7 for a plate spinning about its clamped edge. The plate has a lay-up of [45/−45] with 0.15-mm-thick plies and dimensions of 0.2286 × 0.0762 m. The plate spin axis is parallel to the plate plane and located at the center of its clamped edge. For this ply lay-up, the inclusion of nonlinear terms causes a significant softening, especially in the first torsional mode. At speeds higher than about 430 rpm, the antisymmetry of the plate causes large out-of-plane twisting of the plane taking the plate behavior outside the small-deflection assumption of the present analysis. The linear analysis (incorrectly) shows no such effects.

Figure 8 shows the vibration for a symmetric laminated plate with lay-up $[\pm 22.5/0_2/-22.5/0_2/22.5/0_2]_S$ where the spin axis is parallel to the root edge of the plate and located 0.1667 m from the root of the plate. The plate has dimensions 0.2286 × 0.0762 m and has 0.15-mm-thick plies. The results are compared with Ref. 5. Experimental results were available only for the first three vibration modes. Numerical results are presented for three higher modes also to demonstrate the softening behavior for both the torsional vibration modes. The results show excellent agreement between

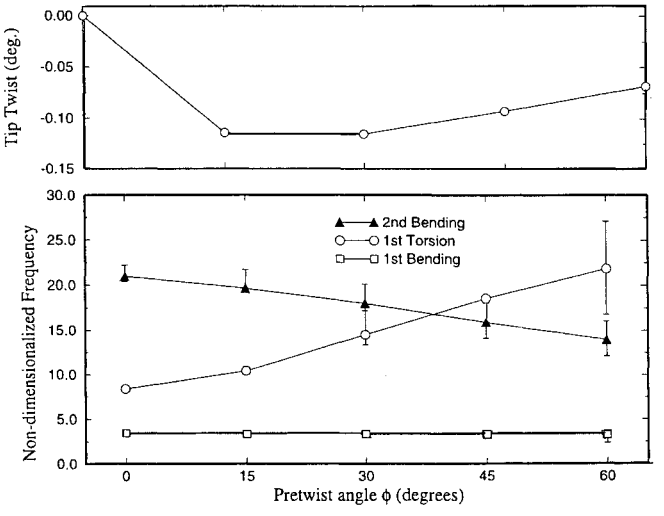

Fig. 6 Nondimensionalized frequencies: pretwisted cantilever square plate, $a/b = 1$ and $b/h = 20$.

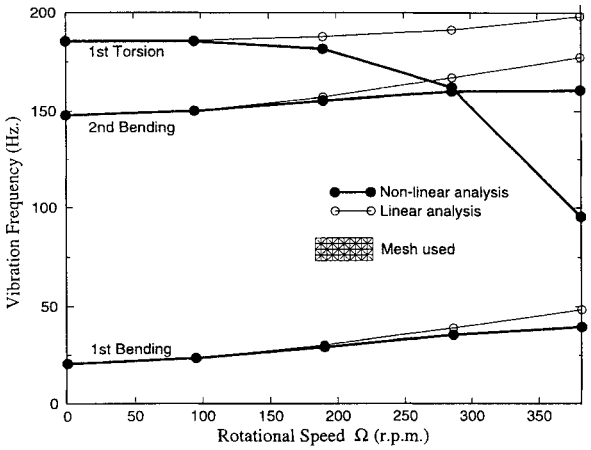

Fig. 7 Effect of inclusion of nonlinear effects on the vibration frequency of a laminated plate [±45].

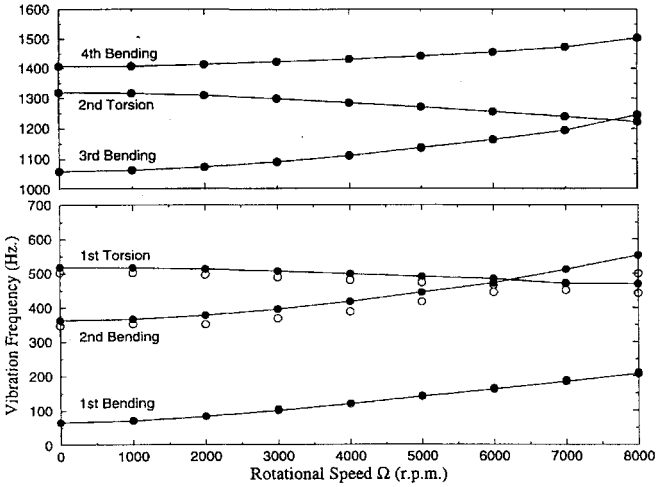

Fig. 8 Vibration of spinning pretwisted composite plate $[\pm 22.5/0_2/-22.5/0_2/22.5/0_2]_S$ twisted about quarter-chord, twist = 30 deg: •, analytical and ○, experimental.

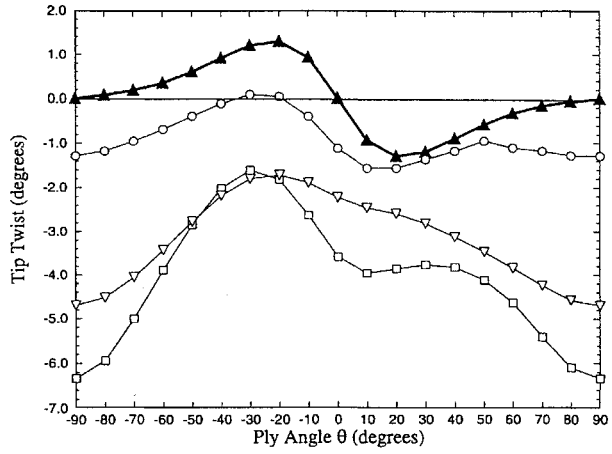

Fig. 9 Effect of unsymmetry on twist of a laminated plate $[\theta_6/0_8/-\theta_6]$ spinning at 5000 rpm: ▲, flat; ○, 5-deg pretwist; □, 15-deg pretwist; and ▽, 30-deg pretwist.

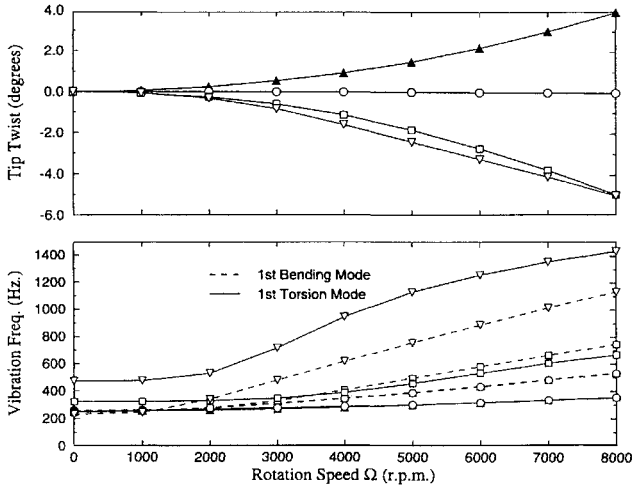

Fig. 10 Effect of unsymmetry on static and dynamic behavior of a rotating laminated plate $[-30_6/0_8/30_6]$: ▲, flat; ○, 5-deg pretwist; □, 15-deg pretwist; and ▽, 30-deg pretwist.

analytical and experimental behavior. For the first bending mode, the experimental and analytical data lie virtually on top of each other and cannot be differentiated in the graph. The vibration behavior of a spinning pretwisted plate is distinct from that for the spinning flat plates since for pretwisted plates the torsional vibration modes show a decrease in frequency with increasing speed. This is because of geometry effects where the centrifugal forces attempt to untwist the plate, bringing its behavior closer to that for flat plates that have lower torsional and higher bending stiffness. This decrease in torsional stiffness causes the torsional frequency to go below the corresponding bending frequency at high rotation speeds. This also results in instability at higher speeds, although, for the plates studied, laminate failure occurs before any such instability is apparent.

Figure 9 shows the effect of unsymmetry on the twisting of the free edge in a spinning plate. A laminated composite plate is studied with an asymmetric stacking sequence $[\theta_6/0_8/-\theta_6]$ and spinning at 5000 rpm. This plate is designed to induce extension-twist coupling ($B_{16} \neq 0$). Thus the plate will twist or untwist as result of the centrifugal force. It is seen that for a flat plate the free edge experiences a positive twist for θ less than zero and a negative twist (untwisting) for θ greater than zero. This behavior is the result of the material extension-twist coupling. As the plate is given an initial pretwist, it is seen that this causes a further geometric coupling between the extension and twist behavior of the plate and results in an increasing value of free edge twist.

The results show that as the initial pretwist increases, there is a corresponding increase in the value of tip twist. However, when the initial pretwist is increased beyond 15 deg, the tip twist starts decreasing. This is similar to the behavior observed in Fig. 6. This behavior is explained by the fact that as pretwist increases, there is an increase in the centrifugal force component twisting the plate edge for low pretwist angles. This force component decreases in magnitude for higher pretwist angles. Also, there is an increase in the torsional stiffness of the plate that overcomes the twisting effect of the centrifugal force. This effect was earlier observed in Ref. 19. It is seen that the twisting of the free edge depends solely on the unsymmetry for a flat plate because of the absence of any geometric coupling in the bend-twist-extension behavior of the plate. But for a pretwisted plate, the geometry causes coupling that offsets or augments the twisting caused by unsymmetry. It is seen that correct ply lay-ups can be selected to minimize the effect of pretwist on the twisting of the free edge (for example 5-deg pretwist, $\theta = -20$ and -35 deg).

Figure 10 shows the effect of unsymmetry on the static and the dynamic behavior of a rotating laminated composite plate with ply lay-up $[-30_6/0_8/30_6]$. This corresponds to $\theta = -30$ deg in Fig. 9. It is seen that besides the expected higher torsion frequency for plates with pretwist, the stiffening effect is even more significant as the rotation speed is increased. The effect of pretwist is not as significant for the bending mode. The figure shows the free edge twist due to centrifugal forces acting on the plate. It is seen that, as expected, for this particular lay-up, the pretwist in the plate tends to offset the effects of material asymmetry. Consequently, in the flat plate the centrifugal forces cause a positive free edge twist that increases with increasing revolutions per minute. On the other hand, for plates with pretwist, the free edge twist decreases and then attains negative twist values with increasing pretwist. For a 5-deg pretwisted plate

this shows that the effects of material unsymmetry and pretwist tend to almost exactly offset each other, resulting in a negligible free edge twist. This is an excellent example to demonstrate that optimum values can be selected for parameters like pretwist and material lay-up to obtain desirable static and dynamic behavior.

VI. Conclusions

Nonlinear finite element techniques were developed to study the nonlinear static deflection and vibration behavior of spinning pretwisted plates made out of composite materials. A six-node triangular finite element was developed to overcome deficiencies in existing elements used for analysis of very thick to very thin laminated composite plates. Results were presented to show the effects of pretwist, laminate ply lay-up, and rotational speed on the behavior of spinning pretwisted plates. The triangular element developed in this study was shown to have better convergence and accuracy than existing finite elements. It was shown that it was important to include nonlinear effects in the analysis of spinning structures to capture change in torsional stiffness behavior. It was shown that desirable static and dynamic behavior can be obtained by selecting optimum values for parameters like pretwist and material lay-up.

Appendix: Mass, Coriolis, and Centrifugal Stiffness Matrices

The linear stiffness matrix $[K_L]$, the nonlinear stiffness matrix $[K_{NL}]$, the geometric stiffness matrix $[K_G]$, and the shear stiffness matrix $[K_G]$ are given as

$$[K_0] = \int_A [B_0]^T [\bar{D}][B_0]\,dA \tag{A1}$$

$$\left[K_e^{NL}\right] = \int_A [B_0]^T [\bar{D}][B_{NL}]\,dA \tag{A2}$$

$$\left[K_e^G\right] = \int_A [B_G]^T \begin{bmatrix} N_x & N_{xy} \\ N_{xy} & N_y \end{bmatrix} [B_G]\,dA \tag{A3}$$

$$\left[K_e^S\right] = \int_a [B_S]^T [\bar{A}][B_S]\,dA \tag{A4}$$

The element stiffness matrix $[K_e^{CF}]$, the element mass matrix $[M_e]$, the element Coriolis matrix $[C_e]$, and the element force vector $\{F_e^{CF}\}$ associated with the centrifugal effects are given as

$$\left[K_e^{CF}\right] = \int_A [N]^T \left[\bar{K}_e^{CF}\right][N]\,dA \tag{A5}$$

$$[M_e] = \int_A [N]^T [\bar{M}_e][N]\,dA \tag{A6}$$

$$[C_e] = \int_A [N]^T [\bar{C}_e][N]\,dA \tag{A7}$$

$$\left\{F_e^{CF}\right\} = \int_A [N]^T \left\{\bar{F}_e^{CF}\right\} dA \tag{A8}$$

where

$$[\bar{M}_e] = \begin{bmatrix} I_1 & 0 & 0 & I_2 & 0 \\ 0 & I_1 & 0 & 0 & I_2 \\ 0 & 0 & I_1 & 0 & 0 \\ I_2 & 0 & 0 & I_3 & 0 \\ 0 & I_2 & 0 & 0 & I_3 \end{bmatrix} \tag{A10}$$

$$[\bar{C}_e] = \begin{bmatrix} 0 & -2I_1\Omega_z & 2I_1\Omega_y & 0 & -2I_2\Omega_z \\ 2I_1\Omega_z & 0 & -2I_1\Omega_x & 2I_2\Omega_z & 0 \\ -2I_1\Omega_y & 2I_1\Omega_x & 0 & -2I_2\Omega_y & 2I_2\Omega_x \\ 0 & -2I_2\Omega_z & 2I_2\Omega_y & 0 & -2I_3\Omega_z \\ 2I_2\Omega_z & 0 & -2I_2\Omega_x & 2I_3\Omega_z & 0 \end{bmatrix} \tag{A11}$$

$$\left\{\bar{F}_e^{CF}\right\} = \begin{Bmatrix} I_1\left[\left(\Omega_y^2 + \Omega_z^2\right)(h_x + x) - \Omega_z\Omega_x h_z - \Omega_y\Omega_x(h_y + y)\right] \\ I_1\left[\left(\Omega_z^2 + \Omega_x^2\right)(h_y + y) - \Omega_z\Omega_y h_z - \Omega_x\Omega_y(h_x + x)\right] \\ I_1\left[\left(\Omega_x^2 + \Omega_y^2\right)h_z - \Omega_y\Omega_z(h_y + y) - \Omega_x\Omega_z(h_x + x)\right] \\ I_2\left[\left(\Omega_y^2 + \Omega_z^2\right)(h_x + x) - \Omega_z\Omega_x h_z - \Omega_y\Omega_x(h_y + y)\right] \\ I_2\left[\left(\Omega_z^2 + \Omega_x^2\right)(h_y + y) - \Omega_z\Omega_y h_z - \Omega_x\Omega_y(h_x + x)\right] \end{Bmatrix} \tag{A12}$$

where

$$(I_1, I_2, I_3) = \sum_{m=1}^{n} \int_{z_m}^{z_{m+1}} \rho^{(m)}(1, z, z^2)\,dz$$

The terms $[N]$ and $[B_G]$ are the matrix of shape functions and the geometric strain-displacement matrix, respectively, given as

$$[N] = \begin{bmatrix} \phi & 0 & 0 & 0 & 0 \\ 0 & \phi & 0 & 0 & 0 \\ 0 & 0 & \chi & 0 & 0 \\ 0 & 0 & 0 & \phi & 0 \\ 0 & 0 & 0 & 0 & \phi \end{bmatrix}, \qquad [B_G] = \begin{bmatrix} 0 & 0 & \chi_{,x} & 0 & 0 \\ 0 & 0 & \chi_{,y} & 0 & 0 \end{bmatrix}$$

Acknowledgments

The continuing support of the current study by the Structural Dynamics Branch of NASA Lewis Research Center and by the San Diego Supercomputer Center is gratefully acknowledged.

$$\left[\bar{K}_e^{CF}\right] = \begin{bmatrix} -I_1\left(\Omega_y^2 + \Omega_z^2\right) & I_1(\Omega_y\Omega_x) & I_1(\Omega_z\Omega_x) & -I_2\left(\Omega_y^2 + \Omega_z^2\right) & I_2(\Omega_y\Omega_x) \\ I_1(\Omega_y\Omega_x) & -I_1\left(\Omega_x^2 + \Omega_z^2\right) & I_1(\Omega_z\Omega_y) & I_2(\Omega_y\Omega_x) & -I_2\left(\Omega_x^2 + \Omega_z^2\right) \\ I_1(\Omega_x\Omega_z) & I_1(\Omega_z\Omega_y) & -I_1\left(\Omega_x^2 + \Omega_y^2\right) & I_2(\Omega_x\Omega_z) & I_2(\Omega_y\Omega_z) \\ -I_2\left(\Omega_y^2 + \Omega_z^2\right) & I_2(\Omega_y\Omega_x) & I_2(\Omega_x\Omega_z) & -I_3\left(\Omega_y^2 + \Omega_z^2\right) & I_3(\Omega_y\Omega_x) \\ I_2(\Omega_y\Omega_x) & -I_2\left(\Omega_x^2 + \Omega_z^2\right) & I_2(\Omega_y\Omega_z) & I_3(\Omega_y\Omega_x) & -I_3\left(\Omega_x^2 + \Omega_z^2\right) \end{bmatrix} \tag{A9}$$

References

[1]Zickel, J., "Bending of Pretwisted Beams," *Journal of Applied Mechanics*, Vol. 22, No. 3, 1955, pp. 348–352.

[2]MacBain, J. C., "Vibrating Behavior of Twisted Cantilever Plates," *Journal of Aircraft*, Vol. 12, No. 3, 1975, pp. 343–349.

[3]Sreenivasamurthy, S., and Ramamurti, V., "Letters to the Editor: Effect of a Tip Mass on the Natural Frequencies of a Rotating Pre-Twisted Cantilever Plate," *Journal of Sound and Vibration*, Vol. 70, No. 4, 1980, pp. 598–601.

[4]Sreenivasamurthy, S., and Ramamurti, V., "A Parametric Study of Vibration of Rotating Pre-Twisted and Tapered Low Aspect Ratio Cantilever Plates," *Journal of Sound and Vibration*, Vol. 76, No. 3, 1981, pp. 311–328.

[5]Lapid, A. J., Kosmatka, J. B., and Mehmed, O., "Behavior of Spinning Laminated Composite Plates with Initial Twist—Experimental Vibrations, Strain and Deflection Results," *A Collection of Technical Papers, AIAA/ASME/ASCE/AHS/ASC 34th Structures, Structural Dynamics and Materials Conference*, Vol. 1, AIAA, Washington, DC, 1993, pp. 255–265.

[6]Tessler, A., and Hughes, T. J. R., "A Three-Node Mindlin Plate Element with Improved Transverse Shear," *Computer Methods in Applied Mechanics and Engineering*, Vol. 50, No. 1, 1985, pp. 71–101.

[7]Yuan, F. G., and Miller, R. E., "A Cubic Triangular Finite element for Flat Plates with Shear," *International Journal for Numerical Methods in Engineering*, Vol. 28, No. 1, 1989, pp. 109–126.

[8]Kosmatka, J. B., "A Reliable Six-Node Triangular Plate/Shell Element for the Analysis of Laminated Composite Structures," *A Collection of Technical Papers, AIAA/ASME/ASCE/AHS 29th Structures, Structural Dynamics and Materials Conference*, AIAA, Washington, DC, 1988, pp. 911–920.

[9]Kosmatka, J. B., "An Accurate Shear-Deformable Six-Node Triangular Plate Element for Laminated Composite Structures," *International Journal for Numerical Methods in Engineering*, Vol. 37, No. 3, 1994, pp. 431–455.

[10]Reissner, E., "The Effect of Transverse Shear Deformation on the Bending of Elastic Plates," *Journal of Applied Mechanics*, Vol. 12, No. 1, 1945, pp. 69–77.

[11]Mindlin, R. D., "Influence of Rotatory Inertia and Shear on Flexural Motions of Isotropic, Elastic Plates," *Journal of Applied Mechanics*, Vol. 18, No. 1, 1951, pp. 31–38.

[12]Whitney, J. M., "A Modified Shear Deformation Theory for Laminated Anisotropic Plates," *Proceedings of American Society for Composites Fifth Technical Conference*, ASC, Washington, DC, 1990, pp. 469–478.

[13]Bhumbla, R., and Kosmatka, J. B., "Stability of Spinning Shear-Deformable Laminated Composite Plates," *Journal of Sound and Vibration*, Vol. 163, No. 1, 1993, pp. 83–99.

[14]Gallagher, R. M., *Finite Element Analysis Fundamentals*, Prentice–Hall, Englewood Cliffs, NJ, 1975.

[15]Guyan, R. J., "Reduction of Stiffness and Mass Matrices," *AIAA Journal*, Vol. 3, No. 2, 1965, p. 381.

[16]Zienkiewicz, O. C., *The Finite Element Method*, McGraw–Hill, New York, 1977.

[17]Bhumbla, R., Kosmatka, J. B., and Reddy, J. N., "Free Vibration Behavior of Spinning Shear-Deformable Plates Composed of Composite Materials," *AIAA Journal*, Vol. 28, No. 11, 1990, pp. 1962–1970.

[18]Kielb, R. E., Leissa, A. W., and MacBain, J. C., "Joint Research Effort on the Vibrations of Twisted Plates, Phase I: Final Results," NASA Reference Publication 1150, June 1985.

[19]Kosmatka, J. B., "On the Behavior of Pretwisted Beams with Irregular Cross-Sections," *Journal of Applied Mechanics*, Vol. 59, 1992, pp. 146–152.

SPACE AND ITS EXPLORATION

J.D. Rummel (U.S.) and V.A. Kotelnikov, M. V. Ivanov (Russia), editors

Volume I in the Space Biology and Medicine series

This is the first book in an important new five-volume series, entitled Space Biology and Medicine. The series is a joint U.S./Russian publication edited by Arnauld E. Nicogossian and Stanley R. Mohler (U.S.), and Oleg G. Gazenko and Anatoliy I. Grigoryev (Russia).

This volume is divided into four parts: Part I, Historical Perspective; Part II, The Space Environment; Part III, Life in the Universe; and Part IV, Space Exploration. Chapter contributions were made by both U.S. and Russian authors. The book also features an Appendix of Astronomical and Physical Quantities, a detailed Subject Index, and an 8–page color section.

1993, 338 pp, illus, Hardback
ISBN 1-56347-061-6
AIAA Members $69.95
Nonmembers $99.95
Order #: 61-6(945)

Future volume titles include:

Volume II—Life Support and Habitability

Volume III—Humans in Space Flight (2 books)

Volume IV—Crew Health, Performance, and Safety

Volume V—Reference Material

Place your order today! Call 1-800/682-AIAA

AIAA
American Institute of Aeronautics and Astronautics

Publications Customer Service, 9 Jay Gould Ct., P.O. Box 753, Waldorf, MD 20604
FAX 301/843-0159 Phone 1-800/682-2422 9 a.m. - 5 p.m. Eastern

Sales Tax: CA residents, 8.25%; DC, 6%. For shipping and handling add $4.75 for 1-4 books (call for rates for higher quantities). Orders under $100.00 must be prepaid. Foreign orders must be prepaid and include a $20.00 postal surcharge. Please allow 4 weeks for delivery. Prices are subject to change without notice. Returns will be accepted within 30 days. Non-U.S. residents are responsible for payment of any taxes required by their government.